arXiv:cond-mat/0412118v2 [cond-mat.supr-con] 16 Dec 2004

On the Relation between Optical Conductivity and Quasiparticle Dynamics: Boson Structures

J.P. Carbotte,[1] E. Schachinger,[2,*] and J. Hwang[1]
[1]*Department of Physics and Astronomy, McMaster University, Hamilton, Ontario, L8S 4M1 Canada*
[2]*Institute of Theoretical and Computational Physics Graz University of Technology, A-8010 Graz, Austria*

(Dated: February 2, 2008)

An extended Drude form is often used to analyze optical data in terms of an optical scattering rate and renormalized mass corresponding, respectively, to the real and imaginary part of the memory function. We study the relationship between memory function and quasiparticle self energy for an isotropic system. We emphasize particularly boson signatures. We find it useful to introduce a new auxiliary model scattering rate and its Kramers-Kronig transform determined solely from optics which are much closer to the self energy than is the memory function itself in the normal state. In the superconducting state the simplification fails because the quasiparticle density of states acquires an essential energy dependence.

PACS numbers: 74.20.Mn 74.25.Gz 74.72.-h

I. INTRODUCTION

Optical[1,2] and angular resolved photo emission (ARPES) data[3,4,5] have given a wealth of information on quasiparticle dynamics in the cuprates both in their normal and superconducting state. The methods are complementary but the exact quantitative relationship between the two is complex. One important difference is that ARPES gives direct information on angular variations around the Fermi surface while optics involves an average over all the quasiparticles participating in the absorption. Even if these anisotropies are not accounted for (isotropic system) there remain additional differences which have their fundamental origin in the fact that ARPES measures directly the quasiparticle spectral density $A(\mathbf{k},\omega)$ at fixed quasiparticle momentum $\mathbf{k}$ as a function of energy ω while optics involves the current-current correlation function which depends on the product of two spectral densities[6,7] at the same momentum $\mathbf{k}$ but with frequencies displaced by the photon energy.

In this paper we focus on similarities as well as on essential differences between the information that is derived from these two different probes and particularly on how they are to be compared. We will be interested in both, the normal and the superconducting state at zero and at finite temperature. In the literature on optics it is the temperature and frequency dependence of the optical scattering rate $\tau_{op}^{-1}(T,\omega)$ which has been particularly emphasized.[2] More recently the imaginary part[8] of the memory function[9,10] related to $\tau_{op}^{-1}(T,\omega)$ by Kramers-Kronig (KK) transform has also been used to compare directly with the energy dependence of the real part of the quasiparticle self energy determined by ARPES.[11,12] Of particular interest in such a comparison is the relationship between the position in frequency of peak structures seen in these quantities and how they reflect corresponding peaks in the electron-boson spectral density $I^2\chi(\omega)$.[13,14,15] For phonons $I^2\chi(\omega)$ is the well known electron-phonon spectral density while in the cuprates exchange of spin fluctuations[7,16,17,18] is more appropriate although as yet there exists no consensus[19] on this issue. Here we will consider several models for $I^2\chi(\omega)$ within an extended Eliashberg formalism. In the superconducting state provision is made for d-wave symmetry of the gap. To keep things simple the same form of $I^2\chi(\omega)$ is used in both gap and renormalization channels but with different magnitudes with the ratio between the two equal to g.

In Sec. II we consider only the normal state and coupling of quasiparticles to a single (ω_E) Einstein mode.[6,20] We also employ a simplified approximate scattering time formulation of the optical conductivity formula in the normal state. This allows some analytic results to be established and provides the motivation for introducing a new model scattering rate and its KK-transform determined solely from optical data but which is very close to the self energy itself. While the real part of the self energy has a logarithmic singularity at ω_E the imaginary part of the memory function does not. Instead, it shows a peak at $\omega = \sqrt{2}\omega_E$. On the other hand, our model quantities reproduce well the self energy at $T=0$ and only very small differences arise at finite T. In Sec. III we provide the more general formalism needed to treat the conductivity accurately as well as to take care of extended $I^2\chi(\omega)$ spectra and the superconducting state. Results in these cases are presented in Sec. IV. For the superconducting state additional complications arise because of the essential energy dependence of the self consistent quasiparticle density of states (DOS). In Sec. V we present our numerical results for our new model scattering rate based on the complete formula for the optical conductivity and solutions of the Eliashberg equations and compare these with the imaginary part of the quasiparticle self energy. We confirm the previous expectation, based on simplifying assumptions, that in the normal state these two quantities are close in magnitude as well as frequency dependence. In the superconducting state they are not. Finally, conclusions are found in Sec. VI.

II. NORMAL STATE AND COUPLING TO A SINGLE BOSON

A generalized Drude form with frequency dependent optical scattering rate $\tau_{op}^{-1}(\omega)$ and optical effective mass ratio $[m^*(\omega)/m]_{op}$ has been used extensively to analyze optical data in a one component approach. The optical conductivity $\sigma(\omega)$ is written in terms of the memory function[9] $M(\omega) = \tau_{op}^{-1}(\omega) - i\omega\lambda_{op}(\omega)$ with $\lambda_{op}(\omega) = \{[m^*(\omega)/m]_{op} - 1\}$ the optical mass renormalization parameter. We have[12]

$$\sigma(\omega) = \sigma_1(\omega) + i\sigma_2(\omega) = \frac{\Omega_p^2}{4\pi}\frac{i}{i\tau_{op}^{-1}(\omega) + \omega\left[1 + \lambda_{op}(\omega)\right]} \tag{1}$$

and $\tau_{op}^{-1}(\omega)$ and $i\omega\lambda_{op}(\omega)$ are related by Kramers Kroning, so that when the optical scattering rate is known, the optical mass renormalization can be obtained from the KK-transform.

The conductivity is a two particle property given by the current-current correlation function. It is related in a complicated way to the quasiparticle self energy (a one particle property) $\Sigma(\omega)$. In the normal state[13] at zero temperature ($T = 0$)

$$\sigma(\omega) = \frac{\Omega_p^2}{4\pi}\frac{i}{\omega}\int_0^\omega d\nu\,\frac{1}{\omega + i\tau_{imp}^{-1} - \Sigma(\nu) - \Sigma(\omega-\nu)}, \tag{2}$$

where τ_{imp}^{-1} is the impurity scattering rate and $\Sigma(\nu)$ accounts for the inelastic scattering. In terms of the electron-phonon or electron-spin fluctuation spectral density $\alpha^2F(\omega)$ or $I^2\chi(\omega)$ respectively[24,25] [call it $F(\omega)$]

$$\begin{aligned}\Sigma(\omega) &= \Sigma_1(\omega) + i\Sigma_2(\omega) = \int_0^\infty d\Omega\,F(\Omega)\ln\left|\frac{\Omega-\omega}{\Omega+\omega}\right| \\ &\quad -i\pi\int_0^{|\omega|} d\Omega\,F(\Omega). \end{aligned}\tag{3}$$

For coupling to a single Einstein mode $F(\omega) = A\delta(\omega - \omega_E)$ we obtain the simple, well known formula

$$\Sigma(\omega) = A\ln\left|\frac{\omega_E - \omega}{\omega_E + \omega}\right| - i\pi A\theta(|\omega| - \omega_E), \tag{4}$$

with $\theta(x)$ the Heavyside θ-function. It is clear from (4) that the imaginary part has a finite jump at ω_E as well as a logarithmic singularity in its real part which can be used to identify boson structure in both cases. The self energy can in principle be determined from ARPES data which measures the quasiparticle spectral function

$$A(\mathbf{k},\omega) = -\frac{1}{\pi}\mathrm{Im}G(\mathbf{k},\omega + i0^+), \tag{5}$$

with the Greens function $G(\mathbf{k},\omega + i0^+) = [\omega - \varepsilon_{\mathbf{k}} - \Sigma(\omega + i0^+)]^{-1}$, where $\varepsilon_{\mathbf{k}}$ is the quasiparticle dispersion. A usefull approximate expression for $\tau_{op}^{-1}(\omega)$ was obtained directly in second order perturbation theory by P.B. Allen.[26] It is (for $T = 0$)

$$\tau_{op}^{-1}(\omega) \simeq \frac{2\pi}{\omega}\int_0^\omega dz\,F(z)(\omega - z) + \tau_{imp}^{-1}. \tag{6}$$

Details in the validity of this form, based on numerical evaluation of Eqs. (2) and (3) are found in Refs. 13 and 27. For $\omega > 0$

$$\tau_{op}^{-1}(\omega) = \frac{2\pi A_{tr}}{\omega}(\omega - \omega_E)\,\theta(\omega - \omega_E), \tag{7}$$

where the subscript tr means transport, although for simplicity, here we will not make a distinction between quasiparticle and transport spectral density; in general they are different. (We have set the impurity term equal to zero for simplicity.) Note that this formula is less favorable for the identification of boson structures than is the imaginary part of the self energy. While it is zero for $\omega < \omega_E$ and finite for $\omega \geq \omega_E$ it has no jump at ω_E. Instead, it smoothly increases from its zero value which makes it harder to identify the exact position of ω_E in $\tau_{op}^{-1}(\omega)$. Application of the KK-transform to Eq. (7) gives immediately

$$\omega\lambda_{op}(\omega) = -2A\left(\ln\left|\frac{\omega_E + \omega}{\omega_E - \omega}\right| + \frac{\omega_E}{\omega}\ln\left|\frac{\omega_E^2 - \omega^2}{\omega_E^2}\right|\right) \tag{8}$$

as the optical mass enhancement. This is to be compared with the real part of the quasiparticle self energy, Eq. (4).

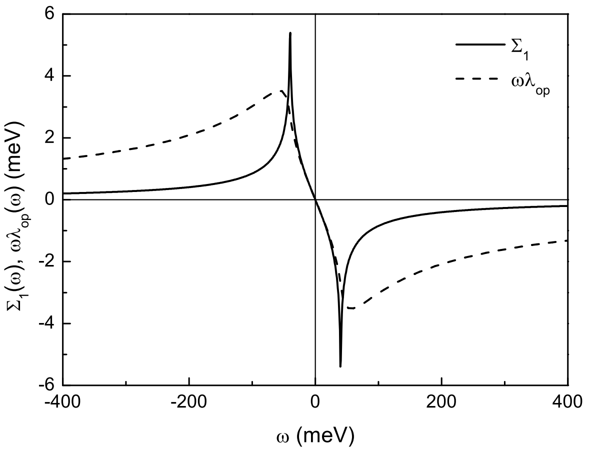

FIG. 1: Comparison of the real part of the quasiparticle self energy $\Sigma_1(\omega)$ as a function of ω with the corresponding optical quantity $\omega\{[m^*(\omega)/m]_{op} - 1\} \equiv \omega\lambda_{op}(\omega)$. Coupling is to a single Einstein oscillator with $\omega_E = 40\,\mathrm{meV}$ and $A = A_{tr} = 1\,\mathrm{meV}$ in Eqs. (4) and (8). There is a logarithmic singularity in $\Sigma_1(\omega)$ at $\omega = \omega_E$ while $\omega\lambda_{op}(\omega)$ only has a small peak at $\omega = \sqrt{2}\omega_E$ and a logarithmic singularity in the slope at $\omega = \omega_E$.

In terms of the usual mass enhancement parameter λ [defined as two times the first inverse moment of $F(\omega)$], $A = \lambda\omega_E/2$, and the limit of $\Sigma_1(\omega)$ as $\omega \to 0$ equals $-\omega\lambda$. Thus the slope of the self energy gives the value of λ as does also $\omega\lambda_{op} \sim \lambda\omega$. This is seen in Fig. 1 where we compare $\Sigma_1(\omega)$ (solid line) and $\omega\lambda_{op}(\omega)$ vs ω (dashed line) for parameters $A = 1\,\mathrm{meV}$ and $\omega_E = 40\,\mathrm{meV}$. While these functions agree in the $\omega \to 0$ limit they deviate from each other at finite frequencies. In particular, at $\omega = \omega_E$ the quasiparticle self energy exhibits a logarithmic singularity while the optical mass renormalization $\omega\lambda_{op}(\omega)$ has only a logarithmic singularity in its slope. It can, furthermore, be shown that $\omega\lambda_{op}(\omega)$ has its maximum at $\omega = \sqrt{2}\omega_E$. Thus, while the boson structure in $\Sigma(\omega)$ appears at the boson energy and is singular, the maximum in $\lambda_{op}(\omega)$ is instead displaced to $\sqrt{2}\omega_E$ and is associated with a rather broad peak in comparison. We conclude from these considerations that the optical mass enhancement parameter $\lambda_{op}(\omega)$ can be used to identify boson structure in the imaginary part of the memory function as done recently by Hwang *et al.*[8] but its signature is much weaker than is the case in the quasiparticle self energy and ω_E is displaced by a factor of $\sqrt{2}$, a fact that does not appear to have been appreciated before, but is important to realize.

In preparation for what will come later when we consider the superconducting state, we note that the self energy (4) and, consequently, the corresponding optical quantity (8) would also apply[21,22,23] in an impurity model with constant quasiparticle scattering rate $\tau_{qp}^{-1} = A$, but in which the normal state quasiparticle density of states, $N(\varepsilon)$, has a gap of size ω_E at the Fermi surface, i.e.: $N(\varepsilon) = N_0$ for $\varepsilon < 0$ and $\varepsilon > \omega_E$ but is zero for $0 < \varepsilon < \omega_E$. This shows immediately that structure in $N(\varepsilon)$ can have an effect on the self energy which is, in some cases, indistinguishable from boson structure. We return to this important point later.

How is this picture changed when we consider finite temperatures? In this case the formulas determining the conductivity as well as the quasiparticle self energy are more complex. Nevertheless, a simple picture still emerges. The normal state optical conductivity is now given by[28]

$$\begin{aligned}\sigma(\omega) &= \frac{\Omega_p^2}{4\pi}\frac{1}{i\omega}\left\{\int_{-\infty}^{0} d\nu\, \tanh\left(\frac{\nu+\omega}{2T}\right) S^{-1}(T,\omega,\nu)\right.\\ &\quad + \int_0^\infty d\nu\left[\tanh\left(\frac{\nu+\omega}{2T}\right) - \tanh\left(\frac{\nu}{2T}\right)\right]\\ &\quad \left.\times S^{-1}(T,\omega,\nu)\right\}, \end{aligned} \tag{9}$$

where

$$S(T,\omega,\nu) = \omega + \Sigma^*(T,\nu+\omega) - \Sigma(T,\nu) - \tau_{imp}^{-1}, \tag{10}$$

and the self energy is[24]

$$\begin{aligned}\Sigma(T,\omega) &= -\int dz\, F(z)\left[\psi\left(\frac{1}{2} + i\frac{\omega+z}{2\pi T}\right)\right.\\ &\quad \left.-\psi\left(\frac{1}{2} + i\frac{\omega-z}{2\pi T}\right)\right], \end{aligned} \tag{11}$$

where $\psi(z)$ is the digamma function and $\Sigma^*(T,\omega)$ is the complex conjugate of $\Sigma(T,\omega)$. For a general $F(z)$

$$\begin{aligned}\tau_{op}^{-1}(T,\omega) &= -2\Sigma_2(T,\omega)\\ &= \pi\int dz\, F(z)\left[2\coth\left(\frac{z}{2T}\right)\right.\\ &\quad \left.-\tanh\left(\frac{\omega+z}{2T}\right) + \tanh\left(\frac{\omega-z}{2T}\right)\right]. \end{aligned} \tag{12}$$

Shulga *et al.*[27] were able to show that to a good approximation

$$\begin{aligned}\tau_{op}^{-1}(T,\omega) &\simeq \frac{\pi}{\omega}\int dz\, F(z)\left[2\omega\coth\left(\frac{z}{2T}\right)\right.\\ &\quad -(\omega+z)\coth\left(\frac{\omega+z}{2T}\right)\\ &\quad \left.+(\omega-z)\coth\left(\frac{\omega-z}{2T}\right)\right]. \end{aligned} \tag{13}$$

At zero temperature Eqs. (12) and (13) reduce to the imaginary part of Eq. (3) and to Eq. (6), respectively. KK-transforms can be used to get from Eqs. (12) and (13) the real part of $\Sigma(T,\omega)$ at finite T as well as $\omega\lambda_{op}(T,\omega)$. Results are shown in Fig. 2 for coupling to a single Einstein mode as in Fig. 1. Three curves are show in each frame. The dotted line applies to the quasiparticle self energy, the dashed line to the corresponding optical quantity and the solid line to a model yet to be defined. The top frames give real parts at $T = 0.1\omega_E$ (left) and at $T = 0.25\omega_E$ (right). The corresponding scattering rates on which these are based, are shown in the two bottom frames. First we consider the top frames. In all cases we see that temperature smooths out the corresponding boson structures, but even for $T = 0.25\omega_E$ they remain easily identifiable, although, the difference between quasiparticle and optical quantities is no longer as pronounced.

The solid curve in Fig. 2 is based on the following observation. At $T = 0$, $d[\omega\tau_{op}^{-1}(\omega)]/d\omega$ given by Eq. (6) equals exactly the quasiparticle scattering rate given as twice the imaginary part of the quasiparticle self energy in Eq. (3). Thus, in this particular limit one can get the quasiparticle scattering rate directly from optics by taking the first derivative of $\omega\tau_{op}^{-1}(\omega)$. Of course, we have assumed that anisotropies in momentum space can be neglected. In general, ARPES will give information on the **k**-dependence of the quasiparticle self energy while optics is always an average. Neglecting such complications, it is interesting to introduce a model scattering

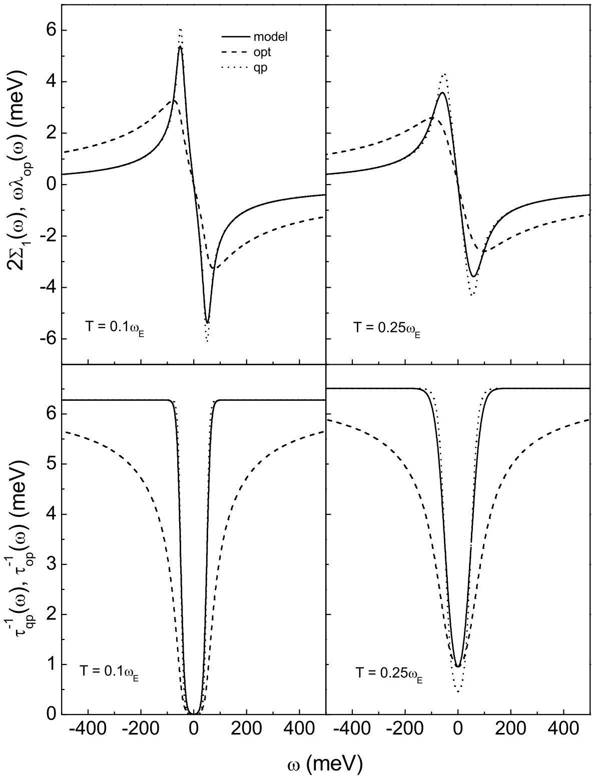

FIG. 2: Top frames give a comparison of the real part of the quasiparticle self energy $2\Sigma_1(\omega)$ (dotted line) with its optical (dashed line) and model (solid line) counterparts as a function of ω. The right hand frame is for temperature $T = 0.25\omega_E$ and the left hand frame is for $T = 0.1\omega_E$. The bottom frames gives corresponding quasiparticle scattering rates on which the results in the two top frames are based. The parameters are $A = 1\,\text{meV}$ and $\omega_E = 40\,\text{meV}$.

rate $\tau^{-1}_{model} \equiv d[\omega\tau^{-1}_{op}(\omega)]/d\omega$ defined from optics alone and consider its relationship to the quasiparticle self energy at finite temperatures. The formula for $\tau^{-1}_{model}(T,\omega)$ equivalent to Eqs. (12) and (13) is

$$\begin{aligned}\tau^{-1}_{model}(T,\omega) &= \pi\int dz\,F(z)\left[2\coth\left(\frac{z}{2T}\right)\right.\\ &\left.+\frac{1-4\left(\frac{\omega-z}{2T}\right)}{\sinh^2\left(\frac{\omega-z}{2T}\right)}-\frac{1-4\left(\frac{\omega+z}{2T}\right)}{\sinh^2\left(\frac{\omega+z}{2T}\right)}\right].\end{aligned} \tag{14}$$

In all cases considered in Fig. 2 the model quantity (solid lines) deviates from its quasiparticle counter part (dotted lines) only very slightly while it deviates much more from the optical case (dashed lines). It is clear, therefore, that if one wishes to compare optical and quasiparticle quantities directly, it is better to use the KK-transform of $\tau^{-1}_{model}(\omega)$ than that for $\tau^{-1}_{op}(\omega)$ itself. The peaks in the corresponding model mass enhancement will now correspond to the Einstein frequency ω_E and it will be sharper than in the optical quantity itself which, as we have seen, is also shifted by $\sqrt{2}$.

Note also, that on comparing top and bottom frame it is the function $\tau^{-1}_{op}(\omega)$ which is least useful in localizing boson structures as discussed in relation to Eq. (7). All the other functions have a sharper signature of the Einstein frequency ω_E.

We next turn to a discussion of how the use of an extended spectrum for $F(\omega)$ modifies our simple results and how the superconducting condensation further modifies boson structures in quasiparticle and optical quantities.

III. EXTENDED BOSON SPECTRUM AND SUPERCONDUCTING STATE

In general, coupling of the electrons to a boson spectrum such as phonons or spin fluctuations is not restricted to a single mode. The corresponding $\alpha^2F(\omega)$ (phonons) or $I^2\chi(\omega)$ (spin fluctuations) can extend to 100 meV or so and even up to 400 meV (of the order of J in the $t-J$ model[29]), respectively. Here we wish to consider such extended spectra and also consider the superconducting state assuming d-wave gap symmetry since we have the cuprates in mind. The equation for $\sigma(\omega)$[30]

$$\sigma(T,\nu) = \frac{\Omega_p^2}{4\pi}\frac{i}{\nu}\left\langle\int\limits_0^\infty d\omega\,\tanh\left(\frac{\beta\omega}{2}\right)[J(\omega,\nu)-J(-\omega,\nu)]\right\rangle_\theta , \tag{15a}$$

where $\langle\cdots\rangle_\theta$ denotes the averaging over angle θ and the function $J(\omega,\nu)$ is given by

$$\begin{aligned}2J(\omega,\nu) &= \frac{1}{E(\omega;\theta)+E(\omega+\nu;\theta)}\,[1-N(\omega;\theta)\\ &\quad\times N(\omega+\nu;\theta)-P(\omega;\theta)P(\omega+\nu;\theta)]\\ &\quad+\frac{1}{E^*(\omega;\theta)-E(\omega+\nu;\theta)}\\ &\quad\times[1+N^*(\omega;\theta)N(\omega+\nu;\theta)\\ &\quad+P^*(\omega;\theta)P(\omega+\nu;\theta)]\,,\end{aligned} \tag{15b}$$

with

$$E(\omega;\theta) = \sqrt{\tilde\omega^2(\omega+i0^+)-\tilde\Delta^2(\omega+i0^+;\theta)}, \tag{15c}$$

and

$$N(\omega;\theta) = \frac{\tilde\omega(\omega+i0^+)}{E(\omega;\theta)}, \qquad P(\omega;\theta) = \frac{\tilde\Delta(\omega+i0^+;\theta)}{E(\omega;\theta)}. \tag{15d}$$

Here E^*, N^*, and P^* are the complex conjugates of E, N, and P, respectively. The two fundamental functions $\tilde\omega(\omega)$ and $\tilde\Delta(\omega)$ are related the renormalization and gap functions, respectively.[7] They are for the gap channel

$$\begin{aligned}
&\tilde{\Delta}(\nu+i0^+;\theta)\\
&\quad=\pi T g\sum_{m=0}^{\infty}\cos(2\theta)\left[\lambda(\nu-i\omega_m)+\lambda(\nu+i\omega_m)\right]\\
&\qquad\times\left\langle\frac{\tilde{\Delta}(i\omega_m;\theta')\cos(2\theta')}{\sqrt{\tilde{\omega}^2(i\omega_m)+\tilde{\Delta}^2(i\omega_m;\theta')}}\right\rangle_{\theta'}\\
&\quad+i\pi g\int_{-\infty}^{\infty}dz\,\cos(2\theta)I^2\chi(z)\left[n(z)+f(z-\nu)\right]\times\\
&\quad\times\left\langle\frac{\tilde{\Delta}(\nu-z+i0^+;\theta')\cos(2\theta')}{\sqrt{\tilde{\omega}^2(\nu-z+i0^+)-\tilde{\Delta}^2(\nu-z+i0^+;\theta')}}\right\rangle_{\theta'},
\end{aligned}\tag{16a}$$

and in the renormalization channel

$$\begin{aligned}
&\tilde{\omega}(\nu+i\delta)\\
&\quad=\nu+i\pi T\sum_{m=0}^{\infty}\left[\lambda(\nu-i\omega_m)-\lambda(\nu+i\omega_m)\right]\\
&\qquad\times\left\langle\frac{\tilde{\omega}(i\omega_m)}{\sqrt{\tilde{\omega}^2(i\omega_m)+\tilde{\Delta}^2(i\omega_m;\theta')}}\right\rangle_{\theta'}\\
&\qquad+i\pi\int_{-\infty}^{\infty}dz\,I^2\chi(z)\left[n(z)+f(z-\nu)\right]\\
&\quad\times\left\langle\frac{\tilde{\omega}(\nu-z+i0^+)}{\sqrt{\tilde{\omega}^2(\nu-z+i0^+)-\tilde{\Delta}^2(\nu-z+i0^+;\theta')}}\right\rangle_{\theta'}.
\end{aligned}\tag{16b}$$

Here

$$\lambda(\nu)=\int_{-\infty}^{\infty}d\Omega\,\frac{I^2\chi(\Omega)}{\nu-\Omega+i0^+}.\tag{16c}$$

The gap is given by

$$\Delta(\nu+i0^+;\theta)=\nu\,\frac{\tilde{\Delta}(\nu+i0^+;\theta)}{\tilde{\omega}(\nu+i0^+)},\tag{16d}$$

or, if the renormalization function $Z(\nu)$ is introduced in the usual way as $\tilde{\omega}(\nu+i0^+)=\nu Z(\nu)$ then

$$\Delta(\nu+i0^+;\theta)=\frac{\tilde{\Delta}(\nu+i0^+;\theta)}{Z(\nu)}.\tag{16e}$$

These equations are a minimum set and go beyond a BCS approach. They include inelastic scattering known to be strong in the cuprate superconductors. In Eq. (16a) g modifies the electron-boson spectral density $I^2\chi(\omega)$ from its value in the renormalized channel. In general the shape of $I^2\chi(\omega)$ could also be different but we have not included this possible complication here.

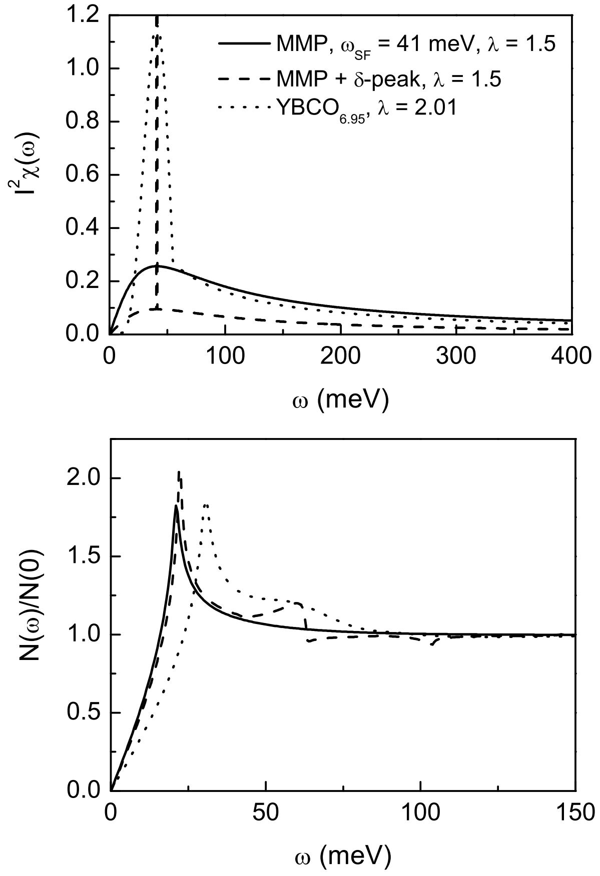

FIG. 3: Top frame: the three models for the electron-boson spectral density $I^2\chi(\omega)$ used in Fig. 4. The MMP model with $\omega_{SF}=41\,\mathrm{meV}$, $\lambda_{MMP}=0.554$ augmented by a δ-function at $\omega_E=41\,\mathrm{meV}$ with $\lambda_\delta=0.946$ for a total of 1.5 (dashed curve). The model spectrum with $\lambda=2.01$ obtained from a fit to the optical conductivity as described in Ref. 16 (dotted curve). Coupling to an optical resonance at 41 meV is included as a peak. A pure MMP spectrum with $\omega_{SF}=41\,\mathrm{meV}$ and $\lambda=1.5$ (solid curve). Bottom frame: the superconducting density of states $N(\omega)/N(0)$ at $T=10\,\mathrm{K}$ for the three spectra shown in the top frame.

In what follows, we will use for $I^2\chi(\omega)$ a form suggested by Millis *et al.*[31] (MMP) given by

$$I^2\chi(\omega)=I^2\,\frac{\omega/\omega_{SF}}{\omega^2+\omega_{SF}^2},\tag{17}$$

with ω_{SF} a spin fluctuation frequency which can be fitted to optical data and to emphasize structure we also will add in one case a δ-function at some specific frequency. Such an MMP form for $\omega_{SF}=41\,\mathrm{meV}$ is shown in the top frame of Fig. 3 (solid line). It has a $\lambda=1.5$. Also shown is the same MMP form now with an added δ-function peak at $\omega_E=41\,\mathrm{meV}$ (dashed line). λ is again equal to 1.5 but now with only 0.554 in the MMP form and the rest in the δ-function. In the superconducting state the MMP form is modified because of the growth of an optical resonance[16,17,18] at 41 meV which is the same frequency at which a spin one resonance is also observed in spin polarized inelastic neutron scattering[32] for optimally doped YBCO. (In other cuprates the position of the observed resonance varies somewhat.[33,34]) This optical resonance grows as the temperature is lowered with the area under the resonance scaling as the superfluid density[7,16] to a reasonable approximation. Such a spectrum has been derived from a fit to $T = 10\,\mathrm{K}$ optical data on a $\mathrm{YBa_2Cu_3O_{6.95}}$ ($\mathrm{YBCO_{6.95}}$) twinned single crystal.[16] This spectrum was also used later on to fit optical data for untwinned single crystals reported by C.C. Homes *et al.*[35,36] and also to calculate the microwave conductivity of the $\mathrm{YBCO_{6.99}}$ single crystals.[37,38] This spectrum is shown as the dotted curve in the top frame of Fig. 3. It has a $\lambda = 2.01$. We will take this $I^2\chi(\omega)$ spectrum as representative of the oxides. Note that coupling to a collective mode at (π,π) is also seen in the ARPES data of Campuzano *et al.*[39] Also note that in the above formulation we have neglected possible momentum space anisotropies. Recent ARPES data by Kaminski *et al.*[40] justify this assumption.

The bottom frame of Fig. 3 shows the quasiparticle density of states $N(\omega)/N(0)$ in the superconducting state for $T = 10\,\mathrm{K}$ for the three spectra presented in the top frame. This would be the classic way to see boson structure in conventional superconductors through tunneling which, so far, has been less successful in the high T_c oxides. This is the reason why optics and ARPES became such important tools in studying the quasiparticle properties. Note that the solid curve for $N(\omega)/N(0)$ which is based on an MMP form with $\omega_{SF} = 41\,\mathrm{meV}$ shows no distinct sharp structure. Thus, a relatively smooth spectrum extending over a large energy scale produces in the quasiparticle density of states only very small, gradual modulations which would be hard but not impossible to detect.

IV. NUMERICAL RESULTS

In Fig. 4 we show our numerical results for the real part of the quasiparticle self energy $\Sigma_1(\omega)$ (only for $\omega > 0$ and made positive) as a function of frequency ω based on numerical evaluation of Eqs. (16) for the renormalized Matsubara frequencies. The black dotted curves apply to the normal and the black solid lines to the superconducting state. Both are at temperature $T = 10\,\mathrm{K}$. The spectrum $I^2\chi(\omega)$ used in the top frame of Fig. 4 is the MMP form of Eq. (8) with $\omega_{SF} = 41\,\mathrm{meV}$ to which we have added a delta function contribution also at $\omega_E = 41\,\mathrm{meV}$. This is shown as the dashed line in the top frame of Fig. 3. The resulting boson structure in the normal state self energy is sharp and falls exactly at $\omega_E = 41\,\mathrm{meV}$. It is the presence of the δ-function in $I^2\chi(\omega)$ which makes the peak so prominent. The corresponding peak in the superconducting state (solid black curve) has shifted to higher frequency and falls slightly below $\omega = \omega_E + \Delta_0 = 63.3\,\mathrm{meV}$ where Δ_0 is the gap amplitude. For an s-wave superconductor the shift in the boson structure would fall exactly at $\omega_E + \Delta_0$ but for d-wave it falls below this value because the gap is distributed in value and we are seeing the result of a distribution of shifts from 0 to Δ_0. The peak has also broadened and the weight under it appears to have increased. In this sense, the opening up of the superconducting gap in the quasiparticle density of states has not only shifted the boson structure but has also, in a sense, enhanced it.

This same statement applies even more strikingly to the corresponding optical quantities. For the imaginary part of the memory function, optical mass renormalization $\lambda_{op}(\omega) = \{[(m^*(\omega)/m] - 1\}$, black dashed curve for the normal state and black dash-dotted curve for the superconducting state, the boson structure is much greater in the dash-dotted curve. Comparing the normal state memory function (black dashed curve) with the self energy (black dotted curve) shows that the structure in the memory function is indeed at $\sqrt{2}\omega_E$ rather than at ω_E although there is a background to our boson spectrum besides the δ-function. This square root of two shift becomes critical in serious comparison ARPES and optical results and has not been appreciated in the past.[8] Note that for the superconducting case the structure in the memory function is greatly enhanced over its normal state value and that it is also shifted upwards in energy as for the self energy. Its exact position depends on the details of the d-wave gap structure and a complete Eliashberg calculation is required to determine it. The size of the peak in the underlying electron-boson spectral density $I^2\chi(\omega)$ is not related simply to the size of the structure seen in the self energy or memory function.

To produce sharp, easily identifiable, structures in ARPES or optical self energies, it is necessary to have correspondingly sharp structures in $I^2\chi(\omega)$. This fact is well illustrated in the bottom frame of Fig. 4 where we show results based on a simple MMP model, Eq. (17), spectral density $I^2\chi(\omega)$ (solid curve in the top frame of Fig. 3). Direct comparison of the curves in the bottom frame of Fig. 4 with the corresponding curves in the top frame shows that now the boson structures are much reduced. Although there is a broad peak at 41 meV in $I^2\chi(\omega)$ for the pure MMP spectrum, this does not translate into a discernable peak in any of our results in the bottom frame of Fig. 4. From this comparison we conclude that a broad peak in $I^2\chi(\omega)$ is difficult to detect as a clear signature in either the real part of the quasiparticle self energy $\Sigma_1(\omega)$ or in the optical mass renormalization $\omega\lambda_{op}(\omega)$ in the normal as well as in the superconducting state. A detailed Eliashberg analysis is needed to extract $I^2\chi(\omega)$ from such data. A method for achieving this has been described in Refs. 16 and 17. An appropriate derivative of $\tau_{op}^{-1}(\omega)$, namely $d^2[\omega\tau_{op}^{-1}(\omega)]/d\omega^2$ which is closely related to $I^2\chi(\omega)$, see Eq. (6), is used to get a first modification to the MMP form, Eq. (16), that fits the optical data better. The procedure can be continued until a reasonable fit with the optical data is obtained from the model spectral density. However, no high accuracy fit has so far been achieved.

In the absence of such an analysis experimentalists have tried to get information on structure in $I^2\chi(\omega)$ through comparison between normal and superconducting state data. To this end we show in the bottom frame of Fig. 4 results for $\omega\lambda_{op}(\omega)$ in the normal state at $T = 90\,\mathrm{K}$ (black dash-double dotted curve). A subtraction of this data from the dash-dotted curve in the superconducting state gives the difference (gray dash-dotted curve). On comparing this curve with the input $I^2\chi(\omega)$ (solid line, top frame of Fig. 3) we see little detail correspondence. The peak in the difference curve is not at 41 meV and the MMP tails at larger values of ω are not picked up. This holds as well if the normal state data at $T = 10\,\mathrm{K}$ (black dashed curve), albeit not accessible to experiment, is used in the subtraction (gray solid curve) or if $\Sigma_1(\omega)$ is considered (gray dotted curve). This subtraction procedure does not give a reliable way to relate boson structure in experimentally measured quantities directly to boson structure in the electron-boson spectral density and is not recommended as an analysis procedure. This is also seen in the middle frame of Fig. 4 which applies to the case of the spectrum fit to optical data on YBCO$_{6.95}$ twinned single crystals.[16] It is shown as the dotted curve in the top frame of Fig. 3. It has a $\lambda = 2.01$ and corresponds to an MMP form modified with an optical resonance peak at $\omega_r = 41$ meV and there is zero weight at small ω. This spectrum is intermediate in "sharpness of boson structure" between the δ-function and the pure MMP case. We see that this reflected itself in how structured $\Sigma_1(\omega)$ and $\omega\lambda_{op}(\omega)$ are. Note in particular that the large peaks in the black dash-dotted curve for $\omega\lambda_{op}(\omega)$ is now shifted to higher frequencies in the middle frame when compared to the top frame although the optical resonance peak is at the same frequency as is the δ-function in Fig. 3. (This is because the gap Δ_0 is bigger now.) This demonstrates once more that no exact correspondence between size and position of the structure in $\omega\lambda_{op}(\omega)$ and $I^2\chi(\omega)$ is possible without a detailed analysis, particularly for extended spectra. Also these functions strongly reflect the energy dependence of the underlying quasiparticle density of states that exists in the superconducting state (dotted curve, bottom frame of Fig. 3) and it is not possible to, so to speak, subtract out the effects of these modulations from the data. Formally the subtraction procedure described above between superconducting and normal state quantities when applied to the middle frame of Fig. 4 again fails to give reliable information on the shape of the boson spectrum.

In the top frame of Fig. 5 we show results for the optical scattering rate $\tau_{op}^{-1}(\omega)$ based on the model $I^2\chi(\omega)$ which consists of an MMP form plus a δ-function (dashed curve in the top frame of Fig. 3) at $\omega_E = 41$ meV. The solid black curve is in the superconducting state at $T = 10\,\mathrm{K}$ while the black dotted curve is in the normal state at the same temperature. While the underlying $I^2\chi(\omega)$ is the same in both cases yet the amount of structure seen in the solid curve is much more pronounced than it is for the dotted curve. This is due entirely to the energy dependence of the quasiparticle density of states (dashed line, bottom frame of Fig. 3) which arises in a d-wave superconductor. On comparing the solid and the dotted curve we note a shift upward in the initial sharp rise in the scattering rate as we go to the superconducting case. This corresponds to the opening of the gap. The black dashed curve is in the normal state at $T = 90\,\mathrm{K}$. Temperature smears the sharp rise at small ω. Only the $T = 90\,\mathrm{K}$ data is available to experiment. If, as we did in Fig. 4, we take the difference between superconducting and normal state optical scattering rate we get the gray solid line for $T = 10\,\mathrm{K}$ and the gray dashed curve for $T = 90\,\mathrm{K}$. The minimum in each of these curves is around 60 meV which is ω_E shifted by approximately Δ_0. It is obviously hard to get reliable information on ω_E from such data. The middle and bottom frames of Fig. 5 are for less structured $I^2\chi(\omega)$ and show a progressive decrease in the corresponding structures in $\tau_{op}^{-1}(\omega)$.

We turn next to the exact correspondence between $\tau_{op}^{-1}(\omega)$ and the quasiparticle scattering rates given as twice the imaginary part of the self energy. In the previous section we have already examined this relation but based our discussion on approximations for the conductivity formula. Next we use the more exact Eq. (15) and solutions of the full Eliashberg equations (16).

V. MODEL SELF ENERGY

We return to the model function $\tau_{model}^{-1}(\omega)$ defined in Sec. III. It can be constructed from the numerical data shown in Fig. 5 for $\tau_{op}^{-1}(\omega)$ defined as

$$\tau_{op}^{-1}(T,\omega) = \frac{\Omega_p^2}{4\pi}\,\mathrm{Re}\,\sigma^{-1}(T,\omega) = \frac{\Omega_p^2}{4\pi}\frac{\sigma_1(T,\omega)}{\sigma_1^2(T,\omega)+\sigma_2^2(T,\omega)}, \tag{18}$$

and

$$\omega\left(\frac{m^*}{m}\right)_{op} = \frac{\Omega_p^2}{4\pi}\,\mathrm{Im}\,\sigma^{-1}(T,\omega) = \frac{\Omega_p^2}{4\pi}\frac{\sigma_2(T,\omega)}{\sigma_1^2(T,\omega)+\sigma_2^2(T,\omega)}. \tag{19}$$

We note in passing, that for small ω the optical effective mass formula (19) is dominated by the imaginary part of the optical conductivity $\sigma_2(T,\omega)$ in the superconducting state because it diverges as ω^{-1} for small ω with coefficients proportional to the inverse square of the penetration depth. This is not related to a quasiparticle effective mass, but is rather a property of the condensate itself. Nevertheless, this is what has been done traditionally and we need to follow this procedure here to make contact with the literature. An alternate approach would be to subtract out of the imaginary part of the optical conductivity the condensate contribution before forming the ratios indicated in Eqs. (18) and (19). In this alternate approach the resulting σ_1 and σ_2 would refer directly only to the normal fluid part of the optical conductivity and so would be more closely related to quasiparticle properties. But this is not what is done in the literature.

For comparison with the quasiparticle self energy it is useful to use $\tau^{-1}_{model}(T,\omega)$ given by

$$\tau^{-1}_{model}(T,\omega) = \frac{\Omega_p^2}{4\pi}\frac{d}{d\omega}\left[\frac{\omega\sigma_1(T,\omega)}{\sigma_1^2(T,\omega)+\sigma_2^2(T,\omega)}\right] \tag{20}$$

than $\tau^{-1}_{op}(T,\omega)$. Its imaginary part is given by the KK-transform

$$\alpha(\omega) = -\frac{1}{\pi}\int_{-\infty}^{\infty} d\omega' \, \frac{\tau^{-1}_{model}(T,\omega')}{\omega'-\omega}. \tag{21}$$

In Fig. 6 we show results for $\tau^{-1}_{model}(\omega)$ based on the numerical results of Fig. 5 and compare directly with the imaginary part of the self energy $\Sigma_2(\omega)$ obtained directly from Eliashberg calculations, namely $\mathrm{Im}\Sigma(\omega) = -\mathrm{Im}\tilde{\omega}(\omega + i0^+)$ of Eq. (16). By definition of the self energy $\tilde{\omega}(\omega + i0^+) = \omega - \Sigma(\omega + i0^+)$. In the two top frames of Fig. 6 we show results for the MMP form (solid line in the top frame of Fig. 3) and in the two bottom frames the YBCO$_{6.95}$ form (dotted curve in the top frame of Fig. 3) for $I^2\chi(\omega)$ is used. In each case we present two frames, the left hand frame is for the normal state and the other frame for the superconducting state. All results are at temperature $T = 10\,\mathrm{K}$. For ease of comparison with $\tau^{-1}_{op}(\omega)$ (dashed lines) it is $\tau^{-1}_{qp}(\omega)/2$ (solid lines) and $\tau^{-1}_{model}(\omega)/2$ (dotted lines) that is shown. Even when a factor of one half is included to make magnitude more comparable, the optical scattering rates differ significantly from the quasiparticle scattering rates. On the other hand, in the normal state the model scattering rate agrees almost perfectly with the quasiparticle scattering rate (top left hand frame). It is clear that $\tau^{-1}_{model}(\omega)$ should be used in comparison with ARPES data and not $\tau^{-1}_{op}(\omega)$. The close correspondence between model and optical rates is, however, lost when the superconducting state is considered (top right hand frame). The solid curve is significantly different from the dotted curve. In particular, $\tau^{-1}_{model}(\omega)$ is smaller at small ω and rises faster around 50 meV after which it stays significantly above its quasiparticle counterpart up to almost 175 meV where the two curves cross again. These differences have their origin in the energy dependence of the superconducting quasiparticle density of states (solid line, bottom frame of Fig. 3) and have nothing to do with the boson structure. For a comparison of $\tau^{-1}_{op}(\omega)$ (optics) and $\tau^{-1}_{qp}(\omega)$ (ARPES) based completely on experiment, the reader is refered to Kaminski *et al.*[41]

When the underlying $I^2\chi(\omega)$ is more structured, as is the case for the YBCO$_{6.95}$ spectrum (dotted curve in Fig. 3), the correspondence between $\tau^{-1}_{model}(\omega)$ and $\tau^{-1}_{qp}(\omega)$ is not as good as is seen in the two bottom frames of Fig. 6. There is a small additional oscillation in the model case, not present in the self energy. Nevertheless, the agreement between them is still much closer than is the case for the optical rate (dashed curve). Note, however, that for the superconducting state the disagreement between $\tau^{-1}_{qp}(\omega)$ (solid curve) and $\tau^{-1}_{model}(\omega)$ (dotted curve) is now much greater and, in particular, a large peak is seen in the model curve which is not there in the dotted curve. This peak can be related to the broad shoulder in the quasiparticle density of states which follows the logarithmic singularity (dotted line, bottom frame of Fig. 3).

VI. CONCLUSION

We have analyzed the relationship between the boson structure seen in the quasiparticle self energy (be it real or imaginary part) measured in ARPES experiments and the corresponding structure seen in the optical memory function determined in the infrared conductivity measurements. Starting first with the real part of the self energy a δ-function peak at $\omega = \omega_E$ in the quasiparticle-boson spectral density $I^2\chi(\omega)$ shows up as a logarithmic-like peak at $\omega = \omega_E$ in the normal state. In the superconducting state a gap develops in the quasiparticle density of states and this introduces further structures in quasiparticle quantities. This effectively shifts to higher energy the normal state boson structure, broadens it, and can make it appear more prominent. For an s-wave gap the shift would be Δ_0 (gap amplitude) but for d-wave it is somewhat less because a distribution of gap values is involved. By contrast, for the memory function the boson structure in the optical mass renormalization is at $\sqrt{2}\omega_E$ in the normal state rather than at ω_E and it is much less prominent. Only a very small peak results which greatly reduces the value of such measurements for determining boson structure as was attempted recently in Ref. 8. Again, the boson structure shifts in the superconducting state and can also appear more prominent as a result of the additional modulation brought about by the opening of a gap. These modifications, however, have nothing to do with the structures in $I^2\chi(\omega)$. The two effects are not additive and require a full non linear Eliashberg analysis to disentangle in detail as we have provided here. When extended rather than δ-function spectra are used, the situation is even more complex. For example, a rather broad peak in $I^2\chi(\omega)$, as in the MMP form for spin fluctuations produces no peak at all, even in the superconducting state.

So far we have described only the real part of the self energy and equivalent optical quantity. Much the same can be said about scattering rates. For a δ-function $I^2\chi(\omega)$, the quasiparticle scattering rate jumps from zero to a finite value at $\omega = \omega_E$ and remains unchanged after that. On the other hand, the optical scattering rate starts from zero at $\omega = \omega_E$ and increases gradually towards the same finite value which it only attains at very high ω. Thus, the signature of a δ-function is not singular as it is for the quasiparticle case.

We have also found that in the normal state a new model scattering rate can be introduced which we denote $\tau^{-1}_{model}(T,\omega)$ and define as $d[\omega\tau^{-1}_{op}(T,\omega)]/d\omega$. It is completely determined from optical data and has the advantage that it follows much more closely the ω dependence of the quasiparticle scattering rate than does $\tau^{-1}_{op}(T,\omega)$ itself. Its KK-transform is very close to the real part of the quasiparticle self energy. We propose that it is this quantity that should be used in comparison between ARPES and optical experimental data. The comparison will be close in isotropic systems and in the anisotropic case, the model quantity gives an average over all directions in the Brillouin zone. In the superconducting state no such simple comparison between ARPES and optics is possible. This needs to be kept in mind when analyzing experimental data, particularly in studies aimed at deriving boson structure from such data. This fact does not seem to have always been appreciated in analysis of experimental data, where features, at least partially associated with the superconducting quasiparticle density of states, has been assigned to boson structure.

The model spectral density $I^2\chi(\omega)$ consisting of an MMP form with superimposed the δ-peak was used to demonstrate that optics as well as ARPES just pick up the sharp structures and do not give direct information on a possible coupling to a smooth background. Nevertheless, it may well be that it is precisely this coupling of the quasiparticles to such a background which is primarily responsible for superconductivity.

Acknowledgment

Research supported by the Natural Sciences and Engineering Research Council of Canada (NSERC) and by the Canadian Institute for Advanced Research (CIAR).

---

[*] Electronic address: schachinger@itp.tu-graz.ac.at; URL: `www.itp.tu-graz.ac.at/~ewald`

[1] D.B. Tanner and T. Timusk, in *Physical Properties of High Temperature Superconductors III*, edited by D.M. Ginsberg (World Scientific, Singapore, 1992), p. 363.

[2] A.V. Puchkov, D.N. Basov, and T. Timusk, J. Phys.: Condens. Matter **8**, 10049 (1996).

[3] J.C. Campuzano, M.R. Norman, and M. Randeria, in *The Physics of Superconductivity Vol. II: Superconductivity in Nanostructures, High-Tc and Novel Superconductors*, edited by K.-H. Bennemann and J.B. Ketterson (Springer-Verlag, Berlin, 2003), Vol. 2, p. 167.

[4] A. Damascelli, Zahid Hussain, and Z.-X. Shen, Rev. Mod. Phys **75**, 473 (2003).

[5] M.R. Norman and C. Pepin, Rep. Prog. Phys **66**, 1547 (2003).

[6] F. Marsiglio and J.P. Carbotte, in *The Physics of Superconductivity Vol. I: Conventional and High-Tc Superconductors*, edited by K.-H. Bennemann and J.B. Ketterson (Springer-Verlag, Berlin, 2003) p. 233.

[7] E. Schachinger and J.P. Carbotte, in: *Models and Methods of High-TC Superconductivity: some Frontal Aspects*, edited by J.K. Srivastava and S.M. Rao, (Nova Science, Hauppauge, NY, 2003), Vol. II, pp. 73.

[8] J. Hwang, T. Timusk, and G.D. Gu, Nature (London) **427**, 714 (2004).

[9] M.A. Quijada, D.B. Tanner, R.J. Kelley, M. Onellion, H. Berger, and G. Margaritondo, Phys. Rev. B **60**, 14917 (1999).

[10] J.W. Allen and J.C. Mikkelsen, Phys. Rev. B **15**, 2952 (1977).

[11] A. Lanzara, P.V. Bogdanov, X.J. Zhou, S.A. Kellar, D.L. Feng, E.D. Lu, T. Yoshida, H. Eisaki, A. Fujimori, K. Kishio, J.-I. Shinoyama, T. Modall, S. Uchida, Z. Hussain, and Z.-X. Shen, Nature (London) **412**, 510 (2001).

[12] X.J. Zhou, T. Yoshida, A. Lanzara, P.V. Bogdanov, S.A. Kellar, K.M. Shen, W.L. Yang, F. Ronning, T. Sasagava, T. Kakeshita, T. Noda, H. Eisaki, S. Uchida, C.T. Lin, F. Zhou, J.W. Xiong, W.X. Ti, Z.X. Zhao, A. Fujimori, Z. Hussain, and Z.-X. Shen, Nature (London) **423**, 398 (2003); E. Cappeluti and L. Pietronero, cond-mat/0309080 (unpublished).

[13] F. Marsiglio, T. Startseva, and J.P. Carbotte, Phys. Lett. A **245**, 172 (1998).

[14] S. Verga, A. Knigavko, and F. Marsiglio, Phys. Rev. B **67**, 054503 (2003).

[15] E. Schachinger, J.J. Tu, and J.P. Carbotte, Phys. Rev. B **67**, 214508 (2003).

[16] E. Schachinger, J.P. Carbotte, and D.N. Basov, Europhys. Lett. **54**, 380 (2001).

[17] J.P. Carbotte, E. Schachinger, and D.N. Basov, Nature (London) **401**, 354 (1999).

[18] E. Schachinger and J.P. Carbotte, Phys. Rev. B **62**, 9054 (2000).

[19] A.V. Chubukov, D. Pines, and J. Schmalian, in *The Physics of Superconductivity Vol. I: Conventional and High-Tc Superconductors*, edited by K.-H. Bennemann and J.B. Ketterson (Springer-Verlag, Berlin, 2003) Vol. 1, p. 495.

[20] J.P. Carbotte, Rev. Mod. Phys. **62**, 1027 (1990).

[21] Mei-Rong Li and J.P. Carbotte, Phys. Rev. B **66**, 155114 (2002).

[22] B. Mitrović and J.P. Carbotte, Can. J. Phys. **61**, 758 (1983); *ibid.* **61**, 784 (1983); *ibid.* **61**, 872 (1983).

[23] B. Mitrović, Ph. D. Thesis, McMaster University 1981 (unpublished).

[24] F. Marsiglio and J.P. Carbotte, Aust. J. Phys. **50**, 975 (1997); *ibid.* **50**, 1011 (1997).

[25] G. Grimvall, *The Electron-Phonon Interaction in Metals*, (North-Holland, New York, 1981).

[26] P.B. Allen, Phys. Rev. B **3**, 305 (1971).

[27] S.V. Shulga, O.V. Dolgov, and E.G. Maksimov, Physica C **178**, 266 (1991).

[28] W. Lee, D. Rainer, and W. Zimmermann, Physica C **159**, 535 (1984).

[29] S. Sorella, G.B. Martins, F. Becca, C. Gazza, L. Capriotti, A. Parola, and E. Dagotto, Phys. Rev. Lett. **88**, 117002 (2002).

[30] J.P. Carbotte and E. Schachinger, Phys. Rev. B (in print).

[31] A. Millis, A.V. Balatsky, and D. Pines, Phys. Rev. B **42**, 167 (1990).

[32] Ph. Bourges, Y. Sidis, H.F. Fong, B. Keimer, L.P. Regnault, J. Bossy, A.S. Ivanov, D.L. Milius, and I.A. Aksay, AIP Conf. Proc. **483**, 207 (1999).

[33] H.F. Fong, P. Bourges, L.P. Regnault, A. Ivanov, G.D. Gu, N. Koshizuka, B. Keimer, Nature (London) **398**, 588 (1999).

[34] H. He, P. Bourges, Y. Sidis, C. Ulrich, L.P. Regnault, S. Pailhès, N.S. Berzigiarova, N.N. Kolesnikov, B. Keimer, Science **295**, 1045 (2002).

[35] E. Schachinger and J.P. Carbotte, Phys. Rev. B **64**, 094501 (2001).

[36] C.C. Homes, D.A. Bonn, R. Liang, W.N. Hardy, D.N. Basov, T. Timusk, and B.P. Clayman, Phys. Rev. B **60**, 9782 (1999).

[37] E. Schachinger and J.P. Carbotte, Phys. Rev. B **65**, 064514 (2002).

[38] A. Hosseini, R. Harris, S. Kamal, P. Dosanjh, J. Preston, R. Liang, W.N. Hardy, and D.A. Bonn, Phys. Rev. B **60**, 1349 (1999).

[39] J.C. Campuzano, H. Ding, M.R. Norman, H.M. Fretwell, M. Randeria, A. Kaminski, J. Mesot, T. Takeuchi, T. Sato, T. Yokoya, T. Takahashi, T. Mochiku, K. Kadowaki, P. Guptasarma, D.G. Hinks, Z. Konstantinovic, Z.Z. Li and H. Raffy, Phys. Rev. Lett. **83**, 3709 (1999).

[40] A. Kaminski, H.M. Fretwell, M.R. Norman, M. Randeria, S. Rosenkranz, J.C. Campuzano, J. Mesot, T. Sato, T. Takahashi, T. Terashima, M. Takano, K. Kadowaki, Z.Z. Li, and H. Raffy, cond-mat/0404385 (unpublished).

[41] A. Kaminski, J. Mesot, H. Fretwell, J.C. Campuzano, M.R. Norman, M. Randeria, H. Ding, T. Sato, T. Takahashi, T. Mochiku, K. Kadowaki, and H. Hoechst, Phys. Rev. Lett. **84**, 1788 (2000).

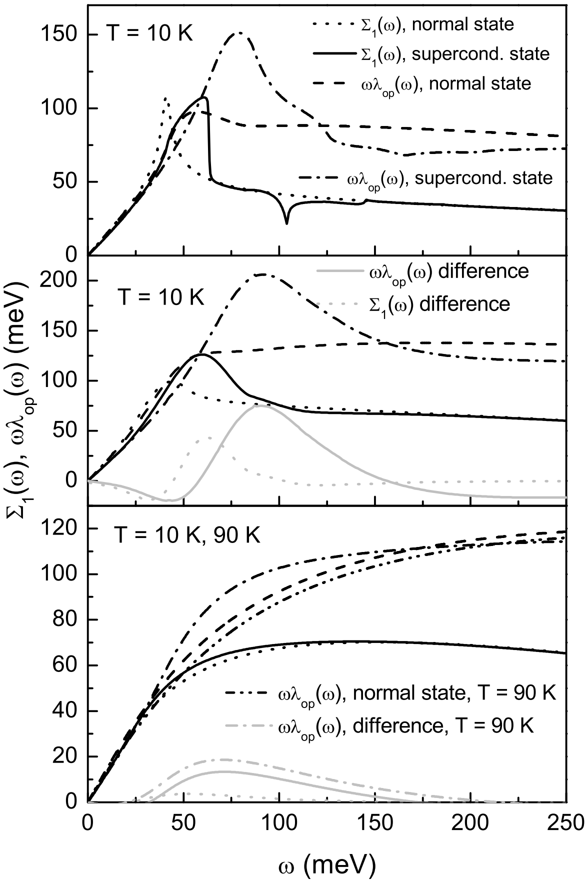

FIG. 4: Comparison of the real part of the quasiparticle self energy $\Sigma_1(\omega)$ vs ω and optical effective mass renormalization $\omega\lambda_{op}(\omega)$ for the three model electron-boson spectral densities $I^2\chi(\omega)$ shown in the top frame of Fig. 3. The top frame is for an MMP form with $\omega_{SF} = 41\,\text{meV}$ and $\lambda_{MMP} = 0.554$ augmented by a δ-function at $\omega_E = 41\,\text{meV}$ with $\lambda_\delta = 0.946$, the middle is obtained with a model $I^2\chi(\omega)$ obtained from consideration of optical properties of YBCO$_{6.95}$ with $\lambda = 2.01$ (dotted curve in the top frame of Fig. 3), and the bottom frame is for the pure MMP with $\omega_{SF} = 41\,\text{meV}$ and $\lambda = 1.5$. In all cases the curves come in pairs $\Sigma_1(\omega)$ in normal (black dotted curve) and superconducting state (black solid curve) and $\omega\lambda_{op}(\omega)$ in normal (black dashed curve) and superconducting state (black dash-dotted curve). In the middle frame we also include as (gray solid line) the difference between superconducting and normal state of $\omega\lambda_{op}(\omega)$ and as gray dotted curve the difference between superconducting and normal state $\Sigma_1(\omega)$. In the bottom frame similar difference curves are shown but with two different values of T in the normal state as labeled.

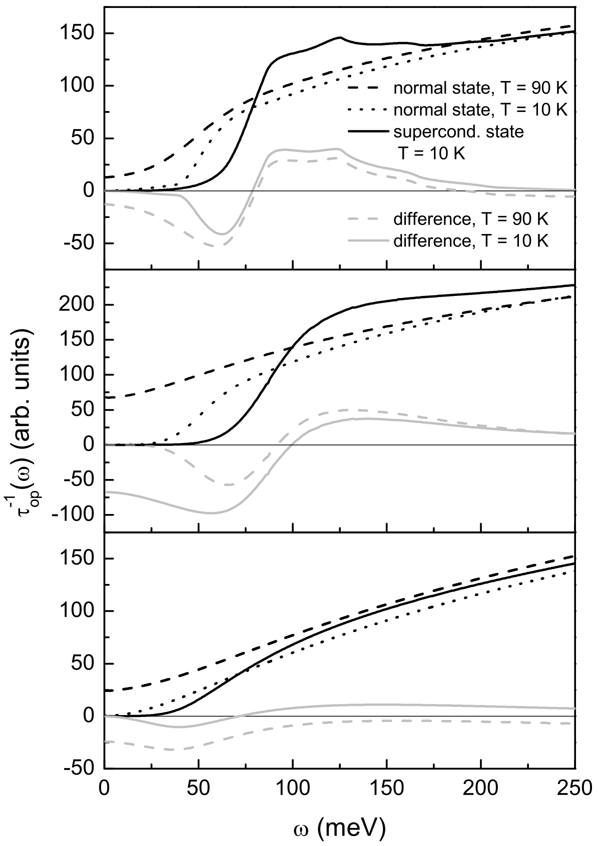

FIG. 5: Optical scattering rates $\tau_{op}^{-1}(T,\omega)$ vs ω for the three quasiparticle-boson spectral densities used in Fig. 4. In each of the three frames the solid black curve is for the superconducting state at $T = 10\,\mathrm{K}$, the black dotted curve for the normal state at the same temperature, and the black dashed curve for the normal state at $T = 90\,\mathrm{K}$. The gray curves are the difference curves, solid curve for $T = 10\,\mathrm{K}$ and dashed curve for $T = 90\,\mathrm{K}$.

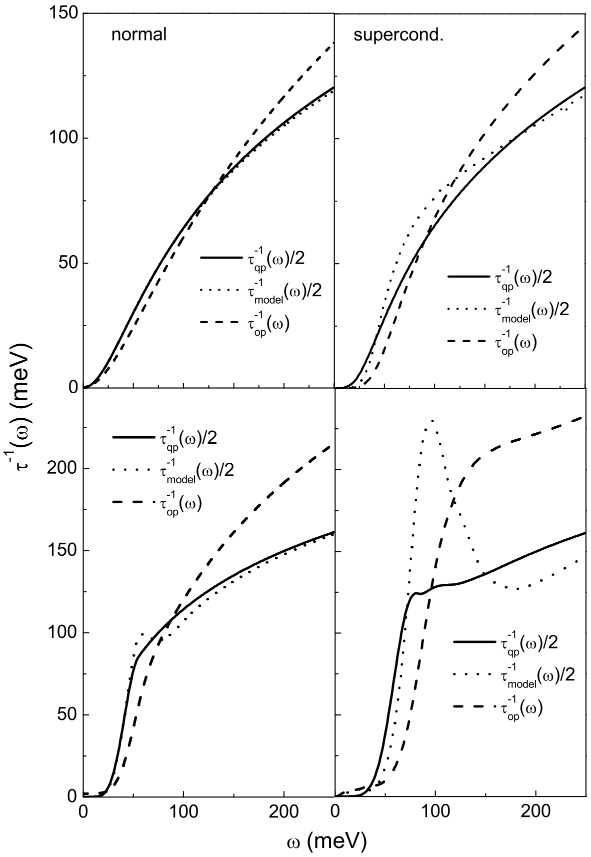

FIG. 6: Comparison of optical, $\tau_{op}^{-1}(\omega)$ (dashed lines), quasiparticle, $\tau_{qp}^{-1}(\omega)$ (solid lines), and model $\tau_{model}^{-1}(\omega)$ (dotted lines) scattering rates vs ω for a temperature of $T = 10\,\mathrm{K}$. For easier comparison $\tau_{qp}^{-1}(\omega)/2$ and $\tau_{model}^{-1}(\omega)/2$ are shown. The two top frames compare our results for an MMP form with $\omega_{SF} = 41\,\mathrm{meV}$ in the normal (left hand frame) and the superconducting state (right hand frame). The two bottom frames give the results for the model $I^2\chi(\omega)$ determined from optics for YBCO$_{6.95}$ as shown in the top frame of Fig. 3 (dotted curve).